ResearchGate

See discussions, stats, and author profiles for this publication at: https://www.researchgate.net/publication/263939759

Molecular-Level Insights into N–N π-Bond Rotation in the pH-Induced Interfacial Isomerization of 5-Octadecyloxy-2-(2-pyridylazo)phenol Monolayer Investigated by Sum Frequency Gener...

ARTICLE *in* THE JOURNAL OF PHYSICAL CHEMISTRY C · JULY 2012

Impact Factor: 4.77 · DOI: 10.1021/jp304023b

CITATIONS
7

READS
59

2 AUTHORS, INCLUDING:

Feng Wei
Jianghan University, Wuhan, China
17 PUBLICATIONS **137** CITATIONS

SEE PROFILE

Available from: Feng Wei
Retrieved on: 31 January 2016

THE JOURNAL OF PHYSICAL CHEMISTRY C

Article

pubs.acs.org/JPCC

Molecular-Level Insights into N−N π-Bond Rotation in the pH-Induced Interfacial Isomerization of 5-Octadecyloxy-2-(2-pyridylazo)phenol Monolayer Investigated by Sum Frequency Generation Vibrational Spectroscopy

Feng Wei and Shuji Ye*

Hefei National Laboratory for Physical Sciences at Microscale, and Department of Chemical Physics, University of Science and Technology of China, Hefei, Anhui, P. R. China 230026

Supporting Information

ABSTRACT: In-situ and real-time characterization of molecular structure of pH stimuli-responsive assembling systems at interfaces is critical to understand the nature of interfacial driving force and weak molecular interaction behind such reactions and provide important clues to control them in a desired manner. In this study, sum frequency generation vibrational spectroscopy (SFG-VS) has been applied, supplemented by surface pressure (π)−area (A) isotherm measurements, and Brewster angle microscopy images, to investigate the interfacial tautomerism and isomerization reactions occurring in 5-octadecyloxy-2-(2-pyridylazo)phenol (PARC18) monolayer at air/buffer solution interface in situ. The isomerization mechanism was examined by measuring interfacial structure of PARC18 molecule at various subphase pH. Time-dependent change of the SFG intensity of the characteristic band was kinetically measured after spreading PARC18 chloroform solution onto different subphase pH buffer solutions. It was found that hydrazone form prevails on the air/water interface in acidic and neutral conditions while azo form dominates at subphase pH $\geq$ 11.6. The hydrazone form adopts a planar geometry at pH = 4.5 and 7.0, whereas the azo form adopts a nonplanar cis or cis-like conformation. It was indicated that the trans−cis isomerization processes follow a rotation mechanism. The deprotonation rate constant was deduced to be 0.20−0.42 M^{-1} s^{-1} at pH = 10.3−12.6. This is the first reported application of SFG-VS to elucidate the isomerization mechanism and deduce the deprotonation rate constant of azoaromatic compounds at interface. Resulting from this study will aid in a better understanding of the interfacial pH-controlled assembly processes.

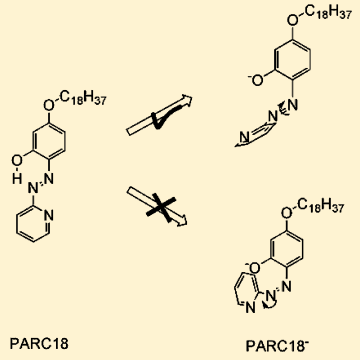

1. INTRODUCTION

pH stimuli-responsive reactions at surfaces and interfaces have attracted increasing interest due to their promising applications in the technology of assembly and catalytic reactions as well as in the nanotechnology for smart controlled surfaces and molecular switches and machines.[1,2] Extensive researches have been performed to pursue development of novelty materials with multifunctional surface properties by using pH stimuli-responsive reactions.[3,4] However, few studies have been carried out to achieve the detailed molecular structure to recognize the nature of driving force and weak molecular interaction behind such reactions. Molecular-level understanding of them will undoubtedly provide important clues to control such reactions in a desired manner.

Azoaromatic compounds are known to be involved in a number of pH stimuli-responsive reactions and considered to be a prototype molecular switch.[5] Amino or hydroxyl group substituted derivatives can respond in a controllable way by pH or photoradiation.[6] The charge dislocation and electronic structure of these molecules can be tuned by pH, resulting in the significant change in the UV−vis absorption spectrum, and the optical properties such as nonlinear susceptibility and photoswitchability.[7] Owing to these performances, azoaromatic compounds associated with polymers and biomolecules have been widely applied to biological systems to study cellular and genetic events.[6,7] These molecules have been designed as amphiphilic molecules to mimic the cellular membrane, polymer/water interface, electrode surface, etc.[6,7]

The azoaromatic compounds usually exist in equilibrium with other tautomeric forms. Hydrazone−azo tautomerism and trans−cis isomerization represent a classical problem in pH stimuli-responsive azoaromatic reactions.[8−11] Although different experimental and theoretical methods have been used to approach this problem,[6−11] the detailed mechanism for the bulk and interfacial isomerization is still an open question. Currently, two controversial mechanisms are under debate:[12−16] one is the rotation mechanism, in which the C−N═N−C dihedral angle changes to isomerize;[17−22] the other is inversion mechanism, in which one N═ N−C bond angle increases to form the isomer, keeping the C−N═N−C atoms planar.[23−25] We believe that direct, in-situ interfacial structural measurements of azo

Received: April 25, 2012
Revised: June 12, 2012
Published: July 3, 2012

 © 2012 American Chemical Society

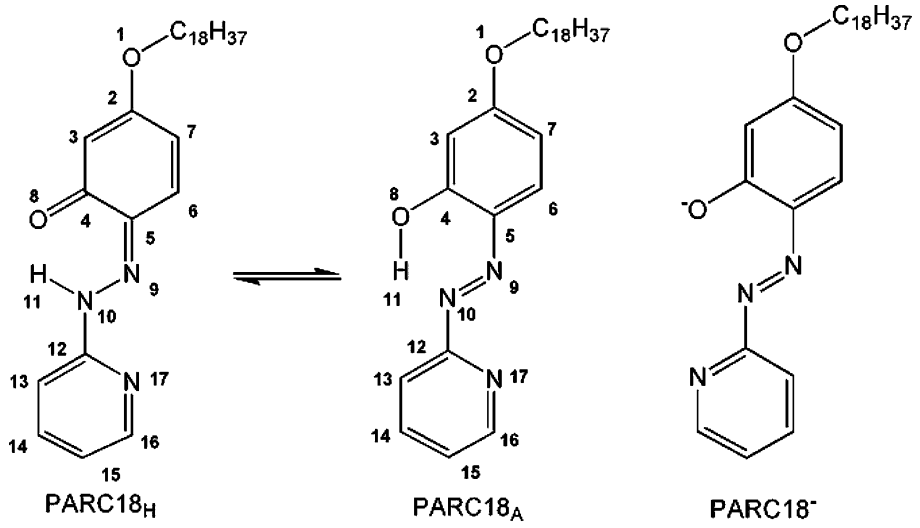

Figure 1. Azo ($PARC18_A$) and hydrazone ($PARC18_H$) tautomer structures of PARC18 molecules at neutral state and deprotonated state ($PARC18^-$).

compounds during isomerization processes will elucidate the precise interfacial isomerization mechanism.

In this research, we applied sum frequency generation vibrational spectroscopy (SFG-VS), supplemented by surface pressure (π)−area (A) isotherm measurements, and Brewster angle microscopy (BAM) images, to investigate the interfacial tautomerism and isomerization reactions occurring in the 5-octadecyloxy-2-(2-pyridylazo)phenol (PARC18, shown in Figure 1) monolayer at various pH values. PARC18 molecules have been demonstrated to be a potential Langmuir−Blodgett film for transition metal ion probing and photorecording.[26−28] SFG-VS is a nonlinear optical laser technique which provides vibrational spectra of surfaces and interfaces.[29−36] It has been applied not only to characterize the molecular structures and orientation of various molecules at surfaces and interfaces[29−36] but also to study the interfacial chemical reactions including interfacial isomerization processes.[37−39] For example, Seki et al. used SFG-VS and density functional calculation to study the structure preference of *trans*- and *cis*-6Az10-PVA monolayer at air/water interface;[37] Wagner et al. investigated the photoisomerization process of CN-Azo-Tripod SAM formed on Au(111) surface;[38] Bonn et al. investigated the interfacial behaviors of photoswitchable lipid DT Azo-5P/DPPC mixtures at air/water interface.[39] On the other hand, π−A isotherm measurements using Langmuir−Blodgett technique offer an illustrative possibility to study the interfacial reaction processes of reactive amphiphilic monolayer at the air/liquid interface.[40] Here we examined the interfacial structure and kinetics of PARC18 molecules by tuning subphase pH in real time in situ. Resulting from this study will provide us some fundamental information to understand the mechanism governing pH stimuli-responsive interfacial isomerization and aid in a better understanding of the interfacial pH-controlled assembly processes.

2. EXPERIMENTAL METHODS

2.1. Chemicals. The sample of PARC18 (purity >99.5%, determined by HPLC) was kindly provided by Prof. Minghua Liu at Institute of Chemistry, CAS. The synthesis and purification procedures were given in the literature.[26−28] The concentration of PARC18 chloroform solution used for the monolayer preparation was 2.1 mM. The salts of sodium phosphate (Na_3PO_4), dibasic and monobasic sodium phosphate (Na_2HPO_4, NaH_2PO_4), sodium chloride (NaCl), and sodium hydroxide (NaOH) were purchased from Alfa Aesar with a purity of >99.0%. All of the chemicals were used as received. The stock salt solution with different pH was prepared by dissolving the salts into ultrapure water from a Milli-Q reference system (Millipore, Bedford, MA). The buffer solution in the pH range of 4.5−12.0 was obtained by mixing different amount of Na_3PO_4, Na_2HPO_4, and NaH_2PO_4, and the solution of pH ≥ 12.0 was controlled by NaCl/NaOH solutions. All of the buffer solutions have the same ionic strength of sodium ions (0.15 M). Monolayer of the PARC18 was formed by spreading a chloroform solution onto a water or buffer solutions surface.

2.2. SFG-VS, Surface Pressure (π)−Area (A) Isotherm Measurements and Brewster Angle Microscopy Experiments. Details regarding SFG theories and measurements have been reported previously.[29−36] The SFG setup is similar to that described in our earlier publications.[41−43] In this research, all SFG experiments were carried out at room temperature (24 °C). The incidence angle at air/water surface is 53° for the IR beam and 63° for the visible beam. The energy of visible beam and IR beam is less than 100 and 100 μJ, respectively. No damage or photoisomerization reactions induced by this energy level have been confirmed. SFG-VS spectra from the interfacial molecules with different polarization combinations including ssp (s-polarized SF output, s-polarized visible input, and p-polarized infrared input) and ppp were collected by overlapping a visible and a tunable IR beam on the sample surface using a copropagating configuration. All SFG spectra were averaged over 200 times at each point and normalized by the intensities of the input IR and visible beams. The energy ratios of IR and visible beams with S/P polarizations were calibrated using a z-cut α-quartz plate. A Langmuir trough was perpendicularly placed to the xz plane of SFG geometry. The surface pressure of PARC18 monolayer was monitored by a BZY-A surface/interface tensiometer (Shanghai Fangrui Instrument CO., Ltd.). The surface area of the monolayer was controlled by a motorized delay stage which is connected to the SMA4 stepper controller of the SFG system. The compressing and detecting

dx.doi.org/10.1021/jp304023b | J. Phys. Chem. C 2012, 116, 16553−16560

procedure was controlled by the software written using labview and is compatible to SFG data acquisition code.

The surface pressure (π)−area (A) isotherm measurements and Brewster angle microscopy experimental details and data analysis methods are presented in the Supporting Information.

3. RESULTS AND DISCUSSION

3.1. Surface Pressure (π)−Area (A) Isotherm Results. Characteristic compression isotherms of PARC18 monolayer at buffer subphase of varying pH are shown in Figure 2A. The

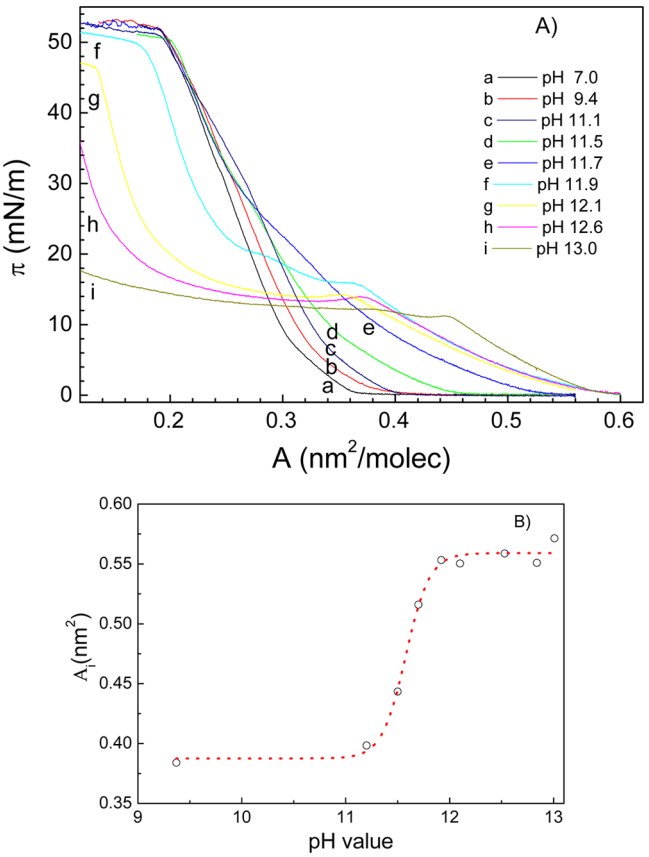

Figure 2. (A) The π−A isotherm of PARC18 monolayers detected at various pH value. (B) The limiting molecular areas derived from π−A isotherm curves as a function of subphase pH; the dotted line is the fitting curve using a sigmoid function with the fitting parameters of $pK_a = 11.6 \pm 0.1$ and $k = 0.11 \pm 0.02$.

isotherms are identical with previous report.[27] After spreading, the PARC18 molecules lie flat on the subphase surface; the (2-pyridylazo)phenol backbone is in contact with the subphase. On the pure DI water and the buffer solution surface of pH ≤ 11.7, the surface pressure monotonically increases during the compression and finally reaches the equilibrium spreading pressure (ESP) of around 52 mN/m, which indicates the monolayer remain in the liquid-expanded state during the course of compression. However, on the buffer solution surface of pH ≥ 11.7, the surface pressure initially grows to a plateau at 11−14 mN/m and then increases slowly. As suggested by recent study,[37] upon the azobenzene molecules converse from the trans form to the cis form, the molecular area is expanded by a factor of ca. 3 at a low surface pressure and the collapse pressure of the cis monolayer is much smaller than that of the trans monolayer. We believe a hydrazone−azo tautomerism and trans−cis isomerization occur at pH ≥ 11.7. This conclusion is further supported by UV−vis absorbance spectra of bulk PARC18 methanol solution (shown in Supporting Information). At pH < 12.1, the absorbance spectrum exhibits an intense π−π^* transition band with λ_{max} at 380 nm. Following pH increasing, the π−π^* transition band blue shifts from 380 to 350 nm, and an absorption band at ∼480 nm becomes more and more intense and finally dominates the spectrum. The band around 480 nm is attributed to an n−π^* transition.[44,45] The appearance of this strong n−π^* absorption band originates from a consequence of an imposed non-planarity between the phenol ring and pyridine ring. It has been well established that the character of the electronic states of azoaromatic compounds critically depend on the planarity between the aromatic groups associated with the azo group.[45−47] The planar trans form allows a strict distinction between π−π^* and n−π^* transitions, while the nonplanar cis form shows a less rigorous distinction because of orbital mixing, thus resulting in a relatively intense n−π^* absorption band and a larger molecular area.[45−47]

By extrapolating the linear part of the π−A isotherm to the zero surface pressure, a limiting area (denoted as A_i) is obtained. For the monolayer of PARC18 on pure water surface, A_i is approximated to 0.36 nm^2/molecule. When PARC18 was spread on the Na_2HPO_4 solution with pH = 9.4, A_i increases to 0.38 nm^2/molecule due to the Hofmeister effect of Na_2HPO_4 in subphase.[28] As the pH increases, A_i starts to increase at pH = 11.2 and then plateaus after pH = 11.7. The phenomenon is further illustrated in Figure 2B, where A_i is plotted as a function of subphase pH. A clear transition is visible within the pH range 11.2−11.7, indicating the molecular geometry of PARC 18 molecules changes. It has been reported that the kinetic and equilibrium constants of many pH-dependent catalytic reaction follow an approximately sigmoid pH−rate profile (eq 1).[48] Figure 2B can be well described by a sigmoid function with the fitting parameters of $pK_a = 11.6 \pm 0.1$ and $k = 0.11 \pm 0.02$. This value of pK_a is slightly lower than the results ($pK_a = 12.2 \pm 0.1$) deduced from the UV−vis absorbance spectra of PARC18/MeOH solution, which is possibly due to the difference between surface and bulk, as well as the different solvent environment.[49]

$$f(\mathrm{pH}) = A_0 + \frac{A_1}{1 + e^{(\mathrm{pH}-pK_a)/k}} \quad (1)$$

3.2. PARC 18 Monolayer Structure at Air/Buffer Solution Interface. *3.2.1. Surface structure at pH = 4.5 and 7.0.* Figure 3 shows SFG spectra PARC18 monolayer at air/buffer solution interface at the subphase pH of 4.5 and 7.0. The spectra were collected from the PARC18 monolayer with surface pressure of ∼26.5 (±2.0) mN/m in the frequency ranging from 1100 −1700 cm^{-1} using the ssp and ppp polarization combinations. BAM results confirm that no aggregation was observed at pH = 4.5−12.6 for this surface pressure level (shown in Supporting Information). The region from 1100 to 1700 cm^{-1} is chosen because it is the "fingerprint" region of (5-octadecyloxy-2-(2-pyridylazo)phenol backbone.

The SFG spectra are dominated by the peaks at 1135, 1200, 1240, 1285, 1330, 1395, 1425, 1440, 1475, 1540, 1575, 1605, and 1635 cm^{-1}. Many proposed assignments for those modes in this class of the molecules have been given in literatures according to Raman spectral features and normal-mode analysis.[45,50−58] However, the assignments exist inconsistencies as a consequence of the complex composition of the normal

dx.doi.org/10.1021/jp304023b | J. Phys. Chem. C 2012, 116, 16553−16560

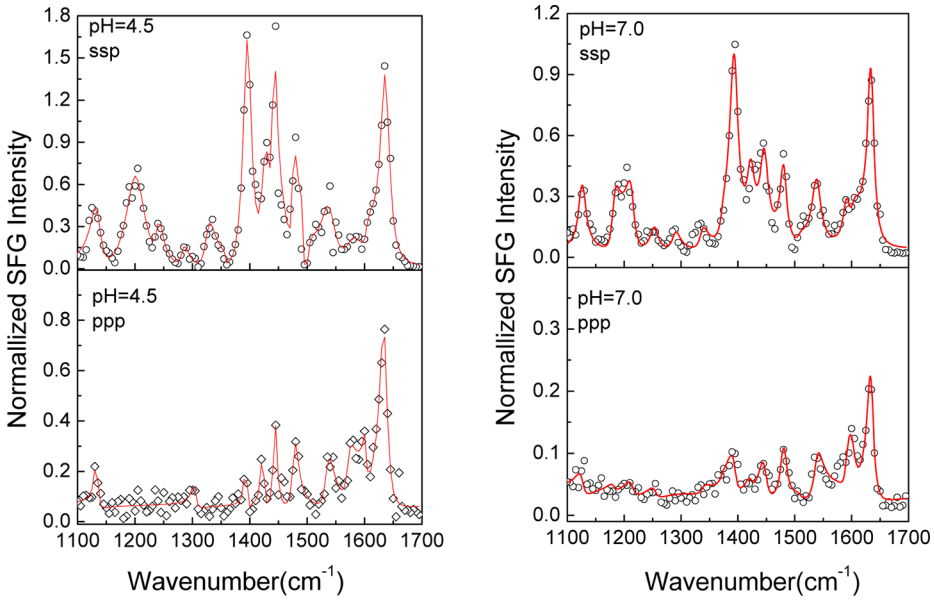

Figure 3. The ssp and ppp SFG spectra of PARC18 monolayer with surface pressure of 26.5(±2.0) mN/m at pH = 4.5 and pH = 7.0.

modes. Based on the existing peak assignments in the literature for the molecules of 4-(2-pyridylazo)resorcinol (PAR) and 4-(2-pyridylazo)naphthol (PAN),[45,50−54] the bands at 1135 and 1285 cm^{-1} originate the stretching of C−N−N═C moiety, whereas the band at 1395 cm^{-1} is attributed to N═N stretching of hydrazone form. The band at 1335 cm^{-1} is assigned to the hybridized mode ν(N¨N) due to hybridization of the N═N and N−N$^-$ bonds. The band at 1635 cm^{-1} arises from the mode ν(C¨O) originating from hybridization of the C═O and C−OH bonds.[53] The presence of those bands provides convincing evidence that hydrazone form prevails at the air/water interface in acidic and neutral conditions. The bands at 1440 and 1475 cm^{-1} result from the ν(C¨C¨C) asymmetric (B_2) and symmetric (A_1) modes of the pyridine ring vibration.[52,59]

3.2.2. Surface Structure at pH = 12.6. Since the hydrazone−azo tautomerism and trans−cis isomerization occur at pH ≥ 11.7, SFG spectra (Figure 4) were also collected from PARC18 monolayer structure with surface pressure of ∼26.5 (±2.0) mN/m at air/buffer solution interface at pH = 12.6 using the ssp and ppp polarization combinations. The spectra collected from the samples at pH = 12.6 are quite different from those at pH = 4.5 and 7.0. At pH = 12.6, the SFG spectra are dominated by the peaks at 1185, 1250, 1285, 1355, 1405, 1470, 1540, and 1600 cm^{-1}. The strong band at 1355 cm^{-1} is contributed by N═N stretching.[45,50−54] Earlier studies have clearly shown that the hydrazone form prevails in acidic and neutral solution.[49] With pH increasing, the tautomeric equilibrium is shifted toward the azo form and then the azo form prevails in alkaline solution, inducing the ν(N═N) mode of PAR shifts from 1390 cm^{-1} at pH 8.0 to 1340 cm^{-1} at pH 14.0.[45,50−54] The absence of the bands at 1125 and 1635 cm^{-1} also suggests that the azo form is the only species present at pH =12.6. An additional notice should be paid to the bands at 1440 and 1475 cm^{-1} in ssp spectra, where the asymmetric (B_2) 1440 cm^{-1} mode disappears while the symmetric (A_1) 1475 cm^{-1} mode has similar intensity with the case at pH = 4.5 and 7.0.

It is worth mentioning that the Raman spectra of azo group in PAR and PAN at pH >12.0 shows a striking similarity with their metal-chelated PAR or PAN complex.[45,51−53] Such

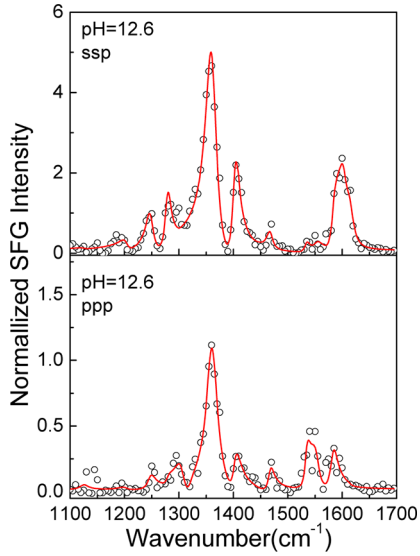

Figure 4. The ssp and ppp SFG spectra of PARC18 monolayer with surface pressure of 26.5 (±2.0) mN/m at pH = 12.6.

similarity implies that PAR and PAN adopt nonplanar geometry at high pH. The SFG results, taking into account π−A isotherm results, and UV−vis absorbance spectra, suggest that hydrazone−azo tautomerism and trans−cis isomerization both occur at high pH. The molecular structure of PARC18 can be thus described by Figure 1. The azo form adopts a nonplanar cis or cis-like conformation.

3.3. Trans−Cis Isomerization Mechanism. In the literature, it is stated that the mechanisms for trans−cis isomerization are under debate:[12−16] one is the rotation mechanism, in which the N−N π-bond is broken and the C−N═N−C dihedral angle changes and isomerizes accompanying a large volume change;[17−22] the other is inversion mechanism, in which the N−N double bond remains intact, and one N═N−C bond angle increases to form the isomer, keeping the C−N═N−C atoms planar.[23−25] The SFG spectra response due to these two mechanisms is different: (1) the frequency of ν(N═N) mode during isomerization has a big shift in the rotation

dx.doi.org/10.1021/jp304023b | J. Phys. Chem. C 2012, 116, 16553−16560

mechanism, whereas the frequency of ν(N═N) mode in trans form is very close to that of the cis form in the inversion mechanism;[24] (2) out-of-plane rotation around the N═N bond occurs without displacing to a large extent the phenyl rings, nor changing the relative orientation of their planes;[18] (3) the rotation mechanism involves in a large change of the twist angle (ψ) of the molecular pyridine ring plane with respect to the surface plane, while the inversion mechanism does not, and thus the SFG intensity of pyridine ring largely depends on the twist angle (ψ) in the rotation mechanism. We believe that it is possible to provide direct evidence on which mechanism best interprets the isomerization processes by analyzing the SFG spectra features of the ν(N═N) mode and the stretch of pyridine ring.

3.3.1. The Peak Shift and Orientation of the ν(N═N) Mode. The ν(N═N) mode of PARC 18 shifts from 1395 cm^{-1} at pH 4.5 and 7.0 to 1355 cm^{-1} at pH 12.6. Apparently, such large frequency shift will involve in the N−N π-bond breaking and then favor to the rotation mechanism. However, there are still some concerns whether the change of orientation angle of the ν(N═N) mode and the twist angle (ψ) of the molecular pyridine ring plane support this mechanism or not.

As introduced in many SFG-VS literatures,[29−36] the molecular orientation information can be obtained by relating SFG susceptibility tensor elements χ_{ijk} (i, j, k = x, y, z) to the SFG molecular hyperpolarizability tensor elements β_{lmn} (l, m, n =a, b, c). If the relation between the χ_{lmn} (l, m, n = s, p) value and orientation angle (θ) of N═N group is given, the orientation angle (θ) of N═N group can be deduced by measuring the ssp and ppp spectral intensity ratio. In a real case, the local symmetry of N═N group is C_{2h}.[18,19,21] For PARC18 molecules, because of the asymmetric connection of phenol ring and pyridine ring, a change in N═N bond length produces a change in the dipole moment, making ν(N═N) mode both be IR- and Raman-active. In addition, the existence of N···H intramolecular hydrogen bonding in PARC18 molecule promotes the formation of planar [n, π] conjugated structure. Such planar structure makes N═N group to have a C_s or $C_{\infty v}$-like symmetric structure. Here we approximate the N═N bond as having $C_{\infty v}$ symmetry. There have been a large number of studies on the orientational analysis for the group with $C_{\infty v}$ symmetry(shown in Supporting Information).[29−35] The parameter R is estimated to be 0.031 by taking the depolarization ratio as 0.30.[23] Under current experimental geometry, the deduced susceptibility ratio $\chi^{(2)}_{ppp}/\chi^{(2)}_{ssp}$ is plotted as a function of orientation angle (θ) in Figure S2. The experimentally measured $\chi^{(2)}_{ppp}/\chi^{(2)}_{ssp}$ of ν(N═N) mode is 0.15 at pH = 4.5 and 7.0 and 0.50 at pH = 12.6, yielding angles of θ = 56° at pH = 4.5 and 7.0 and θ = 51° at pH = 12.6 when a δ-distribution is assumed. The orientation angle changes only 5° (beyond the experimental error). Such a small angle change suggests the isomerization may follow the rotation mechanism. It is worth mentioning that although we assumed the orientation distribution as a δ-distribution, it is in fact very narrow, which has been suggested by the study on Langmuir monolayer of 4′-*n*-octyl-4-cyanobiphenyl and PARC18 by Wang et al.[60,61]

3.3.2. The Twist Angle (ψ) Change of the Molecular Pyridine Ring Plane. It is very interesting to observe that the asymmetric (B_2) 1440 cm^{-1} mode of pyridine ring disappears at pH = 12.6 (Figure 4) while its symmetric (A_1) 1475 cm^{-1} mode has similar intensity with the case at pH = 4.5 and 7.0 (Figure 3). To understand the origin of such spectral feature, we calculate the ssp SFG intensity as a function of the orientation and twist angles of C¨C¨C stretch of pyridine ring by treating C¨C¨C bond as having C_{2v} symmetry (Figure S3 in Supporting Information). The details are given in the Supporting Information. Figure S3 clearly shows that the ssp SFG intensity of B_2 mode largely depends on the twist angle (ψ) for a certain orientation angle (θ) and disappears at ψ = 90°, while the ssp SFG intensity of A_1 mode just decreases a little bit with the increasing twist angle. On the basis of the results of π−A isotherm curves and UV−vis absorbance spectra, the phenol ring and pyridine ring of PARC18 molecules adopt a planar geometry at pH = 4.5 and 7.0. At this case, the twist angle is defined as zero. In addition, the orientation angle of θ = 0° or θ = 90° can be excluded since the signal of A_1 mode at 1475 cm^{-1} does not change markedly. Therefore, the twist angle of the PARC18 molecules at pH = 12.6 is deduced to be approximate to 90° in terms of the indiscernible signals of B_2 mode at 1440 cm^{-1}, indicating the pyridine ring rotates about 90° during the trans−cis isomerization process, which matches quite well with the theoretical prediction (85°−95°).[18,20] This result further supports the rotation mechanism.

3.4. The Real-Time Conformation Change at Different Subphase pH. As discussed above, hydrazone−azo tautomerism and trans−cis isomerization reactions of PARC18 molecules both occur in alkaline solution interface. It is a big challenge on the determination of the kinetics at the air/solution interface. In-situ and real-time characterization of conformation change of PARC18 molecules at interfaces will aid in understanding the interfacial tautomerization and isomerization kinetics. Here we monitored the time-dependent change of the SFG intensity of the characteristic band at 1395 cm^{-1} (I_{ssp}(1395 cm^{-1})) after spreading a 4 μL of PARC18 chloroform solution onto different subphase pH buffer solutions (shown in Figure 5). To avoid the effect of the water surface height on the SFG intensity, a circling pump was used to maintain the water level. After a certain amount of PARC18 solution was spread on surface of the buffer solution with pH = 7.0, I_{ssp}(1395 cm^{-1}) increases to a maximum value in

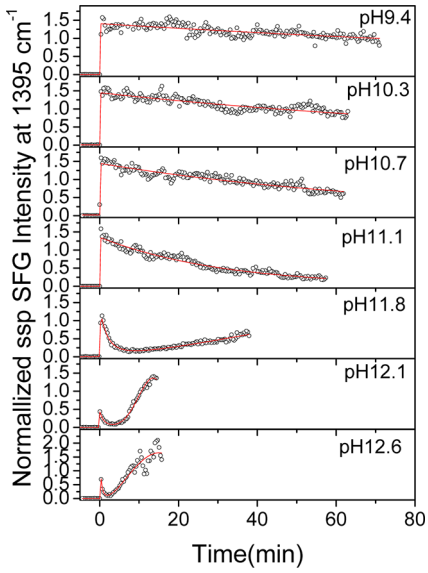

Figure 5. Time dependence of ssp SFG intensity at 1395 cm^{-1} monitored after spreading PARC18 chloroform solution onto different subphase pH buffer solutions.

dx.doi.org/10.1021/jp304023b | J. Phys. Chem. C 2012, 116, 16553−16560

tens of seconds and then keeps almost constant for several hours. For the case on the surface of buffer solution with pH higher than 9.4, $I_{ssp}(1395\ cm^{-1})$ starts to decrease after it reaches the maximum. The decreasing rate is accelerated as pH increases. However, at pH ≥ 11.8, after reaching the maximum, $I_{ssp}(1395\ cm^{-1})$ decreases and then increases again. This transition agrees well with the observation in surface pressure (π)−area (A) isotherms measurements. The spectra measured in the decreasing (Figure 6A) and increasing stage (Figure 6B)

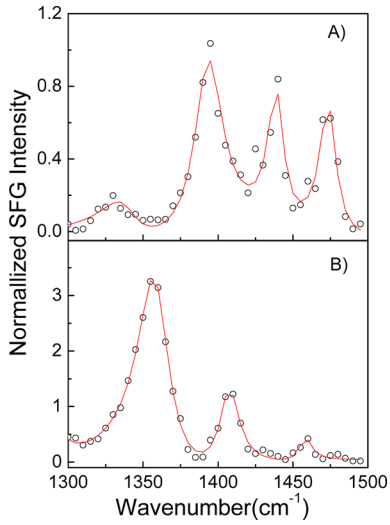

Figure 6. The ssp SFG spectra of PARC18 monolayer after spreading PARC18 chloroform solution onto buffer solutions with subphase pH of pH = 12.6: (A) in the decreasing state shown in Figure 5; (B) in the increasing stage.

at pH = 12.6 confirm that the intensity decrease is mainly caused by the peak shift from 1395 to 1355 cm^{-1} while the intensity increase at pH ≥ 11.8 is attributed to the rise up of the neighboring band at 1405 cm^{-1} of the azo form. Therefore, $I_{ssp}(1395\ cm^{-1})$ as a function of time can be described by followings equations:

$$I_{ssp}(1395\ cm^{-1}, t) \propto |\chi_{ssp}^{1395}(t) + C\chi_{ssp}^{1405}(t) + \chi_{ssp}^{NR}|^2 \quad (2)$$

$$\chi_{ssp}^{1395}(t) \propto N^{H}(t)\chi_{yyz}^{1395}(\theta_1, \psi_1, t) \quad (3)$$

$$\chi_{ssp}^{1405}(t) \propto N^{A}(t)\chi_{yyz}^{1405}(\theta_2, \psi_2, t) \quad (4)$$

where H and A represent hydrazone and azo form. θ and ψ are the polar and azimuthal angle of the corresponding modes. Considering the tautomerism process as a consecutive reaction (eq 5), the molecular number of $N^{H}(t)$ and $N^{A}(t)$ is then given by eqs 6 and 7.

$$\text{hydrazone} + OH^- \xrightarrow{k_1} \text{immediate} \xrightarrow{k_2} \text{azo} \quad (5)$$

$$N^{H}(t) = N^{H}(0)\exp\{-k_1[OH^-]t\} \quad (6)$$

$$N^{A}(t) = N^{H}(0)\left(1 - \frac{k_2}{k_2 - k_1[OH^-]}\exp(-k_1[OH^-]t) + \frac{k_1[OH^-]}{k_2 - k_1[OH^-]}\exp(-k_2 t)\right) \quad (7)$$

where k_1 and k_2 are the rate constants of deprotonation and tautomerism reaction. By substitution of eqs 3, 4, 6, and 7 in eq 2, it is possible to deduce the rate constants of k_1 and k_2 in a crude approximation by fitting the time-dependent change of $I_{ssp}(1395\ cm^{-1})$ and assuming that no reorientations occur to the 1395 and 1405 cm^{-1} modes. Table 1 presents the rate constant of k_1 at different pH value. Excepted that k_1 has a relatively larger value (1.6 s^{-1}) at pH = 9.4, the rate constant of k_1 all falls in the range of 0.20−0.42 $M^{-1}\ s^{-1}$ for pH = 10.3−12.6. This value is several orders of magnitude lower than that of other azoaromatic compounds such as 2-hydroxy-4-methyl-4′-sulfonatazobenzene(varied from 10^6 to 10^9 $M^{-1}\ s^{-1}$ for the pK range 9−12).[62] It is needed to mention that the equilibrium constant (k_1) in eq 7 actually involves in several steps: water interaction, intramolecular hydrogen bonding formation and breaking, and intramolecular rearrangement. Such steps could be the rate-determining step.[63] Earlier study indicated that the step where PAR molecules interact with the surrounding water molecules in the vicinity of the reaction site has a rate constant in the order of 10^{-5}−10^{-6} s^{-1} and increases with the hydrogen-bond strength,[64] which matches well with our result of $k_1[OH^-]$.

4. CONCLUSION

By using SFG-VS and surface pressure (π)−area (A) isotherms measurements, we have investigated the interfacial tautomerism and isomerization reactions occurred in the interfacial PARC18 monolayer at various subphase pH in situ and examined the isomerization mechanism by measuring interfacial structure of PARC18 molecule. In acidic and neutral conditions, hydrazone form prevails on the air/water interface. At subphase pH ≥ 11.6, the azo form dominates. The phenol ring and pyridine ring of hydrazone form adopt a planar geometry at pH = 4.5 and 7.0, while the azo form adopts a nonplanar cis or cis-like conformation. It was found that the trans−cis isomerization processes follow the rotation mechanism. We kinetically measured the time-dependent change of the SFG intensity for the characteristic band after spreading PARC18 chloroform solution onto buffer solutions with different subphase PH. The deprotonation rate constant was deduced to be 0.20−0.42 s^{-1} at pH = 10.3−12.6.

■ ASSOCIATED CONTENT

Supporting Information

UV−vis absorption spectra of PARC18 molecules at different pH, surface pressure (π)−area (A) isotherm measurements, Brewster angle microscopy experimental details, and SFG-VS data analysis methods. This material is available free of charge via the Internet at http://pubs.acs.org.

Table 1. Rate Constants of k_1 as a Function of pH

	pH						
	9.4	10.3	10.7	11.1	11.8	12.1	12.6
$k_1[OH^-]$ (s^{-1})	4.0×10^{-5}	6.9×10^{-5}	1.1×10^{-4}	2.7×10^{-4}	2.5×10^{-3}	5.3×10^{-3}	11.2×10^{-3}
k_1 ($M^{-1}\ s^{-1}$)	1.6	0.35	0.21	0.21	0.40	0.42	0.28

dx.doi.org/10.1021/jp304023b | J. Phys. Chem. C 2012, 116, 16553−16560

AUTHOR INFORMATION

Corresponding Author

*E-mail shujiye@ustc.edu.cn; Tel 086-(551)360-3462; Fax 086-(551)360-3462.

Notes

The authors declare no competing financial interest.

ACKNOWLEDGMENTS

This work was supported by the National Natural Science Foundation of China (Grants 21073175 and 91127042), the National Basic Research Program of China (Grant 2010CB923300), and the Knowledge Innovation Program of the Chinese Academy of Sciences (KJCX2-EW-W09). The authors appreciate that Prof. Minghua Liu provided the PARC18 samples and offered some background of PARC18 LB films. F.W. thanks Prof. Hong-Fei Wang and Prof. Yuan Guo for their kind help and discussions. S.Y. thanks Prof. Yi Luo at USTC for his kind help and discussions.

REFERENCES

(1) Hu, Z. B.; Chen, Y. Y.; Wang, C. J.; Zheng, Y. D.; Li, Y. *Nature* **1998**, *393*, 149−152.
(2) Yu, X.; Wang, Z.; Jiang, Y. G.; Shi, F.; Zhang, X. *Adv. Mater.* **2005**, *17*, 1289−1293.
(3) Chen, T.; Ferris, R.; Zhang, J. M.; Ducker, R.; Zauscher, S. *Prog. Polym. Sci.* **2010**, *35*, 94−112.
(4) Mi, L.; Bernards, M. T.; Cheng, G.; Yu, Q. M.; Jiang, S. Y. *Biomaterials* **2010**, *31*, 2919−2925.
(5) Merino, E. *Chem. Soc. Rev.* **2011**, *40*, 3835−3853.
(6) Lee, H. Y.; Song, X. L.; Park, H.; Baik, M. H.; Lee, D. *J. Am. Chem. Soc.* **2010**, *132*, 12133−12144.
(7) Beharry, A. A.; Woolley, G. A. *Chem. Soc. Rev.* **2011**, *40*, 4422−4437.
(8) Matazo, D. R. C.; Ando, R. A.; Borin, A. C.; Santos, P. S. *J. Phys. Chem. A* **2008**, *112*, 4437−4443.
(9) Dunn, N. J.; Humphries, W. H.; Offenbacher, A. R.; King, T. L.; Gray, J. A. *J. Phys. Chem. A* **2009**, *113*, 13144−13151.
(10) Wang, D.; Dusek, K.; Kopeckova, P.; Duskova-Smrckova, M.; Kopecek, J. *Macromolecules* **2002**, *35*, 7791−7803.
(11) Seki, T.; Fukuchi, T.; Ichimura, K. *Langmuir* **2002**, *18*, 5462−5467.
(12) Wildes, P. D.; Pacifici, J. G.; Irick, G.; Whitten, D. G. *J. Am. Chem. Soc.* **1971**, *93*, 2004−2008.
(13) Asano, T.; Okada, T.; Shinkai, S.; Shigematsu, K.; Kusano, Y.; Manabe, O. *J. Am. Chem. Soc.* **1981**, *103*, 5161.
(14) Rau, H.; Luddecke, E. *J. Am. Chem. Soc.* **1982**, *104*, 1616.
(15) Tamai, N.; Miyasaka, H. *Chem. Rev.* **2000**, *100*, 1875.
(16) Stuart, C. M.; Frontiera, R. R.; Mathies, R. A. *J. Phys. Chem. A* **2007**, *111*, 12072−12080.
(17) Chang, C.-W.; Lu, Y.-C.; Wang, T.-T.; Diau, E. W.-G. *J. Am. Chem. Soc.* **2004**, *126*, 10109−10118.
(18) Ciminelli, C.; Granucci, G.; Persico, M. *Chem.—Eur. J.* **2004**, *10*, 2327−2343.
(19) Cembran, A.; Bernardi, F.; Garavelli, M.; Gagliardi, L.; Orlandi, G. *J. Am. Chem. Soc.* **2004**, *126*, 3234−3243.
(20) Ciminelli, C.; Granucci, G.; Persico, M. *J. Chem. Phys.* **2005**, *123*, 174317.
(21) Cusati, T.; Granucci, G.; Persico, M. *J. Am. Chem. Soc.* **2011**, *133*, 5109−5123.
(22) Landge, S. M.; Tkatchouk, E.; Benitez, D.; Lanfranchi, D. A.; Elhabiri, M.; Goddard, W. A., III; Aprahamian, I. *J. Am. Chem. Soc.* **2011**, *133*, 9812−9823.
(23) Biswas, N.; Umapathy, S. *J. Chem. Phys.* **1997**, *107*, 7849−7858.
(24) Fujino, T.; Arzhantsev, S. Y.; Tahara, T. *J. Phys. Chem. A* **2001**, *105*, 8123−8129.
(25) Schultz, T.; Quenneville, J.; Levine, B.; Toniolo, A.; Martinez, T. J.; Lochbrunner, S.; Schmitt, M.; Shaffer, J. P.; Zgierski, M. Z.; Stolow, A. *J. Am. Chem. Soc.* **2003**, *125*, 8098−8099.
(26) Liu, M. H.; Ushida, K.; Nakahara, H.; Kira, A. *Adv. Mater.* **1997**, *9*, 1099−1101.
(27) Liu, M. H.; Ushida, K.; Kira, A.; Nakahara, H. *Thin Solid Films* **1998**, *327*−*329*, 491−494.
(28) Ushida, K.; Liu, M. H.; Izumi, Y. *Sep. Sci. Technol.* **1999**, *34*, 359−367.
(29) Shen, Y. R. *The Principles of Nonlinear Optics*; Wiley: New York, 1984.
(30) Gracias, D. H.; Chen, Z.; Shen, Y. R.; Somorjai, G. A. *Acc. Chem. Res.* **1999**, *32*, 930−940.
(31) Wang, H. F.; Gan, W.; Lu, R.; Rao, Y.; Wu, B. H. *Int. Rev. Phys. Chem.* **2005**, *24*, 191−256.
(32) Moore, F. G.; Richmond, G. L. *Acc. Chem. Res.* **2008**, *41*, 739−748.
(33) Richmond, G. L. *Annu. Rev. Phys. Chem.* **2001**, *52*, 357−389.
(34) Castellana, E. T.; Cremer, P. S. *Surf. Sci. Rep.* **2006**, *61*, 429−444.
(35) Lambert, A. G.; Davies, P. B.; Neivandt, D. J. *Appl. Spectrosc. Rev.* **2005**, *40*, 103−145.
(36) Ye, S. J.; Nguyen, K. T.; Le Clair, S.; Chen, Z. *J. Struct. Biol.* **2009**, *168*, 61−77.
(37) Ohe, C.; Kamijo, H.; Arai, M.; Adachi, M.; Miyazawa, H.; Itoh, K.; Seki, T. *J. Phys. Chem. C* **2008**, *112*, 172−181.
(38) Ovari, L.; Schwarz, J.; Peters, M. V.; Hecht, S.; Wolf, M.; Tegeder, P. *Int. J. Mass Spectrom.* **2008**, *277*, 223−228.
(39) Backus, E. H. G.; Kuiper, J. M.; Engberts, J. B. F. N.; Poolman, B.; Bonn, M. *J. Phys. Chem. B* **2011**, *115*, 2294−2302.
(40) Peltonen, J. P. K.; He, P. S.; Linden, M.; Rosenholm, J. B. *J. Phys. Chem.* **1994**, *98*, 12403−12409.
(41) Wei, F.; Xu, Y. Y.; Guo, Y.; Liu, S. L.; Wang, H. F. *Chin. J. Chem. Phys.* **2009**, *22*, 592−600.
(42) Ye, S. J.; Wei, F. *Analyst* **2011**, *136*, 2489−2494.
(43) Ye, S. J.; Liu, G. M.; Li, H. C.; Chen, F. G.; Wang, X. W. *Langmuir* **2012**, *28*, 1374−1380.
(44) Wang, Z.; Cook, M. J.; Nygard, A. M.; Russell, D. A. *Langmuir* **2003**, *19*, 3779−3784.
(45) De Oliveira, L. F. C.; Santos, P. S.; Ribeiro, M. C. C. *J. Raman Spectrosc.* **1997**, *28*, 53−59.
(46) Biswas, N.; Umapathy, S. *J. Phys. Chem. A* **1997**, *101*, 5555−5566.
(47) Suzuki, H. *Electronic Absorption Spectra and Geometry of Organic Molecules*; Academic Press: New York, 1967; Chapter 23.
(48) Coleman, J. E. *Annu. Rev. Biophys. Biomol. Struct.* **1992**, *21*, 441−483.
(49) Ghasemi, J.; Lotfi, S.; Safaeian, M.; Niazi, A.; Mazloum, M. *J. Chem. Eng. Data* **2006**, *51*, 1530−1535.
(50) Trotter, P. J. *Appl. Spectrosc.* **1977**, *31*, 30−35.
(51) Crane, L. G.; Wang, D. X.; Sears, L. M.; Heyns, B.; Carron, K. *Anal. Chem.* **1995**, *67*, 360−364.
(52) Drozdzewski, P. M. *Spectrochim. Acta* **1985**, *41A*, 1035−1039.
(53) Sett, P.; Paul, N.; Brahma, S. K.; Chattopadhyay, S. *J. Raman Spectrosc.* **1999**, *30*, 611−618.
(54) Leopold, N.; Szabo, L.; Aluas, M.; Leopold, L. F.; Chis, V. *J. Mol. Struct.* **2009**, *919*, 94−99.
(55) Matazo, D. R. C.; Ando, R. A.; Borin, A. C.; Santos, P. S. *J. Phys. Chem. A* **2008**, *112*, 4437−4443.
(56) Snehalatha, M.; Ravikumar, C.; Joe, I. H. *Solid State Sci.* **2009**, *11*, 1275−1282.
(57) Munro, C. H.; Smith, W. E.; Armstrong, D. R.; White, P. C. *J. Phys. Chem* **1995**, *99*, 879−885.
(58) Zimmermann, F.; Lippert, Th.; Beyer, Ch.; Stebani, J.; Nuyken, O.; Wokaun, A. *Appl. Spectrosc.* **1993**, *47*, 986−993.
(59) Castellucci, E.; Sbrana, G.; Verderame, F. D. *J. Chem. Phys.* **1969**, *51*, 3762−3770.
(60) Rao, Y.; Tao, Y. S.; Wang, H. F. *J. Chem. Phys.* **2003**, *119*, 5226−5236.

(61) Rao, Y.; Tao, Y. S.; Wang, H. F. *Proc. SPIE* **2003**, *5223*, 177−186.
(62) Rose, M. C.; Stuehr, J. *J. Am. Soc. Chem.* **1971**, *93*, 4350−4354.
(63) Shi, Y. L.; Eyring, E. M.; van Eldik, R. *J. Chem. Soc., Dalton Trans.* **1998**, 3565−3576.
(64) Yoshida, N.; Fujimoto, M. *Bull. Chem. Soc. Jpn.* **1980**, *53*, 101−105.